Biomaterials 181 (2018) 310–317

Contents lists available at ScienceDirect

Biomaterials

journal homepage: www.elsevier.com/locate/biomaterials

Photosensitizer-crosslinked in-situ polymerization on catalase for tumor hypoxia modulation & enhanced photodynamic therapy

Hairong Wang[a], Yu Chao[a], Jingjing Liu[a], Wenwen Zhu[a], Guanglin Wang[b], Ligeng Xu[a], Zhuang Liu[a,*]

[a] Institute of Functional Nano & Soft Materials (FUNSOM), Jiangsu Key Laboratory for Carbon Based Functional Materials and Devices, Soochow University, Suzhou, Jiangsu 215123, China

[b] School of Radiation Medicine and Protection and School for Radiological and Interdisciplinary Sciences (RAD-X) Collaborative Innovation Center of Radiation Medicine of Jiangsu Higher Education Institutions Medical College of Soochow University Suzhou, Jiangsu 21513, China

ARTICLE INFO

Keywords:
In-situ polymerization
Catalase
Tumor hypoxia modulation
Photodynamic therapy

ABSTRACT

Tumor hypoxia is known to be one of critical factors that aggravate the tumor resistance to photodynamic therapy (PDT) in which oxygen is essential for tumor destruction. Herein, catalase, an enzyme to trigger hydrogen peroxide (H_2O_2) decomposition, is modified by in-situ free radical polymerization, using meso-tetra(*p*-hydroxyphenyl) porphine (THPP) as the cross-linker to enable condensed grafting of short polyethylene glycol (PEG) chains on the protein surface as a permeable brush-like safeguard. The formulated catalase-entrapped nanocapsules (CAT-THPP-PEG) with enhanced enzyme stability can be labeled with $^{99m}Tc^{4+}$, a radioisotope ion that is chelated by the porphyrin structure of THPP, to allow in vivo single-photon emission computed tomography (SPECT) imaging. It is found that such CAT-THPP-PEG nanoparticles exhibit efficient tumor passive retention after intravenous injection, and are able to greatly relieve tumor hypoxia by triggering the decomposition of tumor endogenous H_2O_2 into oxygen. With THPP functioning as a photosensitizer, in vivo PDT is further conducted, achieving a remarkable antitumor therapeutic effect. This work presents an enzyme modification strategy by in-situ polymerization with photosensitizer as the cross-linker to develop multifunctional nano-theranostics with strengthened enzymatic stability, efficient tumor passive homing, SPECT imaging capability, enhanced PDT efficacy as well as decreased immunogenicity, promising for clinical translation.

1. Introduction

Tumor hypoxia originated from irregular cancer cell proliferation and distorted tumor vasculatures has been realized to be one of critical characteristics of the poor therapeutic outcomes for many types of cancer treatments, particularly photodynamic therapy (PDT) in which oxygen is a critical element in the process of cancer cell destruction [1–7]. Up to now, several strategies have been developed to overcome tumor hypoxia including promoting intratumor blood flow, delivering oxygen into tumors by oxygen shuttles, and producing oxygen in situ to promote tumor oxygenation, as well as targeting hypoxia induced factors [7–12]. In particular, considering the existence of endogenous hydrogen peroxide (H_2O_2) produced by the aberrant metabolism of cancer cells inside solid tumors, the utilization of H_2O_2-catalysts to decompose the tumor endogenous H_2O_2 into O_2 has been recognized to be an attractive strategy to relieve tumor hypoxia and improve therapeutic efficacy of PDT [13–18].

Catalase (CAT) is a specific catalytic enzyme with an extremely high enzyme turnover number to decompose H_2O_2 into O_2, and has been employed to fabricate several types of nano-theranostics to relieve tumor hypoxia in combination with other therapeutic approaches [19–22]. However, as an exogenous enzyme, the immunogenicity of CAT as well as the protease-induced degradation are non-negligible factors that may limit its in vivo functions after systemic administration due to the complicated physiological environments [23–26]. To date, several efforts on modification of enzymes have been made to improve their in vivo stability and realize tumor-targeted delivery such as encapsulating enzymes within inorganic or polymer nanoparticles to protect them from protease digestion. However, some of those methods may result in the partial loss of the enzymatic activity [27–29]. Moreover, the interaction between enzyme and carriers might be not stable enough in such complicated in vivo environment while the unfavorable escape of enzyme from the capsules may initiate the hostile immunogenicity [30–32]. On the other hand, chemical modification via

* Corresponding author.
E-mail address: zliu@suda.edu.cn (Z. Liu).

https://doi.org/10.1016/j.biomaterials.2018.08.011
Received 26 February 2018; Received in revised form 3 August 2018; Accepted 3 August 2018
Available online 04 August 2018
0142-9612/ © 2018 Elsevier Ltd. All rights reserved.

covalent conjugation provides a reliable route to enhance enzyme stability under the complicated in vivo environment to avoid the directly contact between enzymes and surrounding proteins [33,34]. In particular, the acrylate on the surface of proteins to further enable in situ free radical polymerization has been demonstrated to be a unique strategy for enzyme modification [35–38]. The polymerized thin network and permeable layer can effectively stabilize the interior enzyme, offering a novel class of biocatalytic nanocapsules with outstanding activity and stability for various applications. Therefore, it would be interesting to use this method to modify catalase by incorporating photosensitizers to realize the enhanced tumor PDT by relieving tumor hypoxia.

In this work, by employing meso-tetra(*p*-hydroxyphenyl) porphine (THPP), a photosensitizer, as the crosslinker and short-chained polyethylene glycol (PEG) as the drafting moiety, we develop an in-situ free radical polymerization method to modify CAT, obtaining a unique type of CAT-THPP-PEG nanocapsules. Within this functional system, catalase, which is well protected inside the nanocapsule, is employed as a oxygen generator to decompose endogenous H_2O_2 and produce oxygen, so as to promote the therapeutic efficacy of the oxygen-dependent PDT treatment that is trigged by light illumination of photosensitizer THPP. Besides, the PEG chains polymerized on the surface of catalase would form a permeable brush-like layer which could sterically prevent the direct contact between serum proteins and CAT, and thus enhance the enzyme stability and further diminish its immunogenicity (Fig. 1a) [39–44]. Additionally, by taking advantages of the porphyrin structure of THPP to chelate metal ions, the formed CAT-THPP-PEG nanoparticles can be easily labeled with $^{99m}Tc^{4+}$ for in vivo single-photon emission computed tomography (SPECT) imaging, which reveals efficient tumor retention of those nanoparticles after intravenous (i.v.) injection. Owing to the greatly relieved tumor hypoxia and the capability of THPP as a photosensitizer, effective in vivo PDT cancer treatment is demonstrated in a mouse tumor model experiment. Therefore, this work presents a facile way to prepare a unique type of enzyme entrapped theranostic nanocapsules for enhanced cancer therapy via modulating tumor hypoxia, promising for translational nanomedicine.

2. Results and discussion

Enzyme encapsulated nanoparticles were synthesized via in situ free radical polymerization on the surface of proteins, with catalase (CAT) and bovine serum albumin (BSA) as two examples. As shown in Fig. 1a, CAT or BSA was firstly pre-modified with acryloyl groups, followed by polymerization with acrylated monomer poly(ethylene glycol) methacrylate (PEGMA). Both THPP and N,N′-methylene bis-acrylamide (BIS) were introduced crosslinkers to facilitate the formation of a stable crosslinked structure. In the obtained CAT-THPP-PEG nanocapsules, a brush-like crosslinked PEG protecting shell on the CAT surface would be helpful to keep the enzymatic activity and prevent its direct interaction with other surrounding proteins. As the control, BSA-THPP-PEG nanoparticles were synthesizes by using BSA to replace CAT following the same method. The chemical structure of acryloyl-THPP was confirmed by ^1H NMR spectra (Fig. S1a, Supporting Information) while the concentration of THPP was determined by ultraviolet–visible spectroscopy (UV–Vis) (Fig. S1b, Supporting Information). The synthesized CAT-THPP-PEG nanoparticles showed spherical morphology with an average diameter at ~25 nm (Fig. 1c), while the average hydrodynamic size of those nanoparticles was measured by dynamic light scattering (DLS) to be ~30 nm (Fig. 1b), indicating the successful encapsulation of CAT. Notably, CAT-THPP-PEG nanoparticles showed great stability in different physical solutions including phosphate buffered saline (PBS) as well as fetal bovine serum (FBS), in which negligible difference size change was noticed for those nanoparticles after 24 h incubation (Fig. 1b).

Catalase is known to be an effective catalytic enzyme to decompose H_2O_2 into water and oxygen. It is important for us to evaluate the catalytic capability of CAT since several modifications were taken place on CAT. Herein, the dissolved O_2 generated from enzymatic reaction of CAT-THPP-PEG in H_2O_2 solutions with series concentrations and different pH values was measured by an oxygen probe (JPBJ-608 portable Dissolved Oxygen Meters, Shanghai REX Instrument Factory). It was found that CAT-THPP-PEG nanoparticles still kept the catalytic activity to decompose H_2O_2 into O_2 even at a low H_2O_2 concentration (Fig. 1d), although the relative enzymatic activity of CAT-THPP-PEG was slightly decreased compared with that of free catalase (Fig. S1c, Supporting Information). Moreover, the pH value within the physiological range showed no significant effect on the catalytic efficiency of CAT within CAT-THPP-PEG nanoparticles (Fig. 1e). The dissolved O_2 concentrations under light illumination were also tested at different illumination time intervals (Fig. 1 f). The reduced oxygen concentration under light in our CAT-THPP-PEG system clearly demonstrated the consumption of oxygen in the PDT process. After that, the catalytic capability of CAT-THPP-PEG after light illumination was investigated in Fig. 1g, from which one could know that the light illumination would have no negative effect on the activity of CAT.

Exogenous enzymes often may gradually lose their activities in vivo due to the complicated physiological environment particularly with the existence of proteases. Herein, one of our purposes to prepare catalase encapsulated nanoparticles by the covalent shell is preventing its digestion by proteases. Hence, we evaluated the enzymatic stability of CAT-THPP-PEG nanoparticles compared to naked catalase against protease K by the Góth method [45]. As shown in Fig. 1h, compared to the fast digestion and the rapid loss of enzyme activity for free CAT upon exposure to protease K, CAT-THPP-PEG nanoparticles showed well protected enzyme activity against protease K, with ~60% of activity remained after incubation with protease K for 12 h. The enhanced enzyme stability again protease is a greatly preferred feature for their in vivo application via systemic administration.

To verify the photodynamic therapeutic feasibility of the nanoparticles, the singlet oxygen (SO) generation abilities of CAT-THPP-PEG and BSA-THPP-PEG under 660-nm LED light at the power density of 5 mW cm^{-2} were then determined by electron spin-resonance spectroscopy (ESR) as well as the recovered fluorescence of singlet oxygen sensor green (SOSG), a SO specific dye. The light-triggered SO production by different types of nanoparticles appeared to be rather efficient (Fig. S2 in supporting information), without showing appreciable difference between different formulations at the same THPP concentration as well as the normoxic and hypoxic conditions (Fig. 1i and j). Remarkably, in the presence of H_2O_2 (100 μM), the light-triggered SO production by CAT-THPP-PEG was obviously increased under both normoxic and hypoxic conditions due to the extra oxygen supplied by the CAT-triggered decomposition of H_2O_2. Such a phenomenon was not observed for BSA-THPP-PEG, whose photodynamic SO production was not affected by the H_2O_2. In addition, the SO generation under the hypoxic condition was not as efficient as that under the normoxic condition, also indicating the necessary of O_2 supply in PDT treatment. Hence, it is reasonable to predict that the PDT efficiency would be enhanced inside the tumor where exists a substantial level of endogenous H_2O_2 (50–100 μM) [46].

In vitro experiments were then carried out to evaluate the cancer cell killing ability of such CAT-constructed nanoparticles. Remarkably, the gradually increased fluorescence attributed to THPP could be observed in cells incubated with CAT-THPP-PEG nanoparticles as revealed by confocal laser scanning microscopy (CLSM) images, suggesting the efficient cellular uptake of those nanoparticles by a time-dependent manner (Fig. 2a). Next, the cytotoxicity of CAT-THPP-PEG and BSA-THPP-PEG against 4T1 cells was studied by the methyl thiazolyl tetrazolium (MTT) assay (Fig. 2b), from which no noticeable adverse effects of those nanoparticles to cells could be recognized. Considering the existence of large hypoxic regions within solid tumors, the *in vitro* PDT therapeutic efficacies of CAT-THPP-PEG and BSA-THPP-PEG to

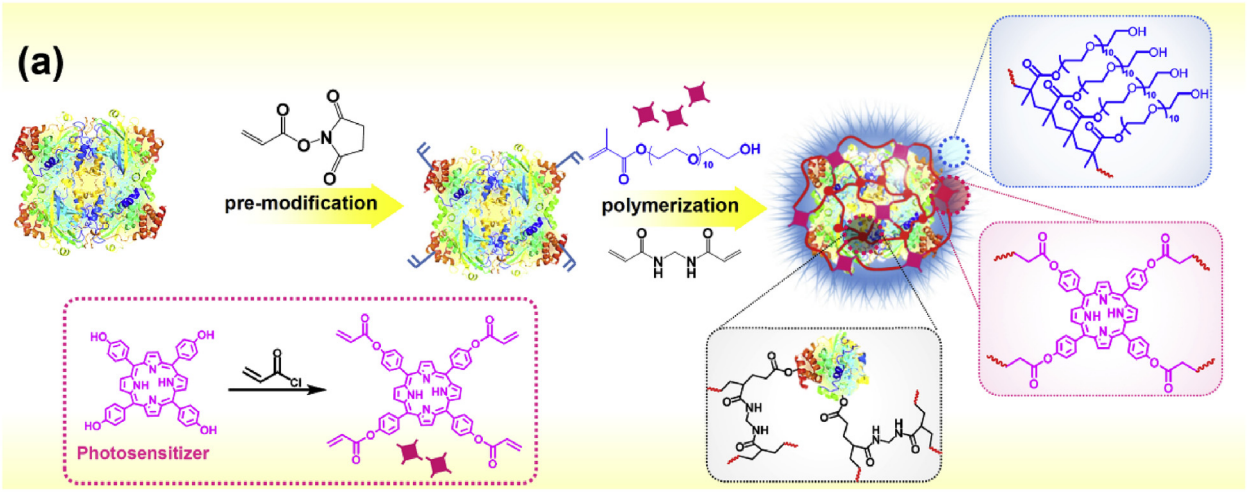

(b)

Sample	Media	Size (nm)	Size PDI
free CAT	1x PBS	5	0.091
CAT-THPP-PEG	water	30	0.155
	1x PBS	28	0.168
	FBS solution	32	0.235
BSA-THPP-PEG	1x PBS	39	0.185

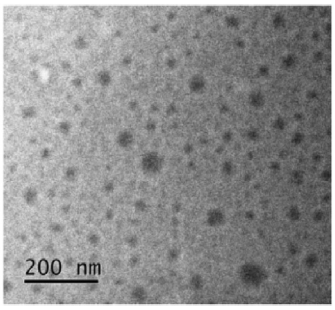

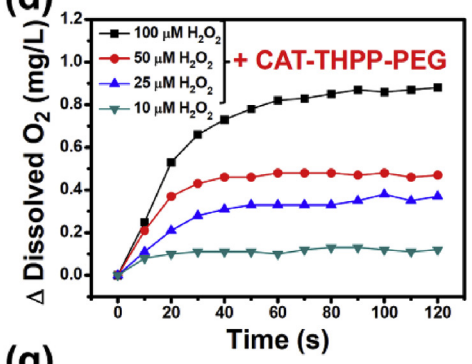

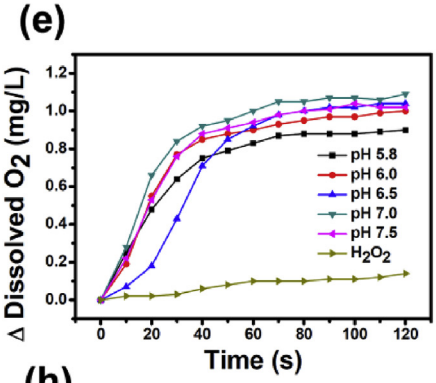

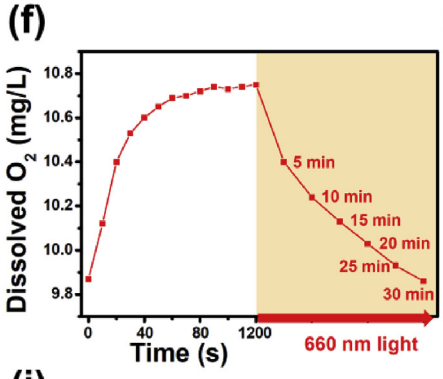

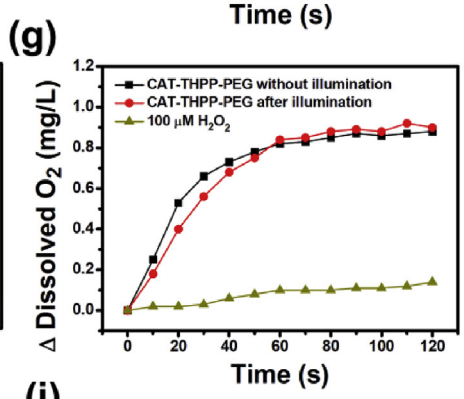

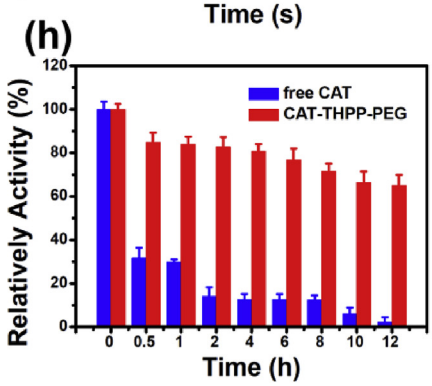

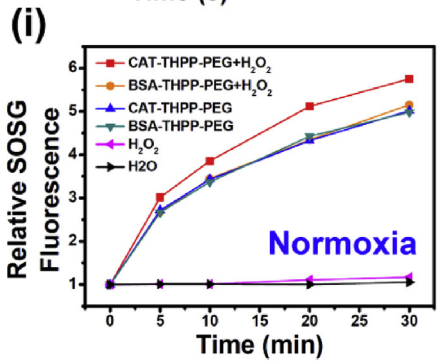

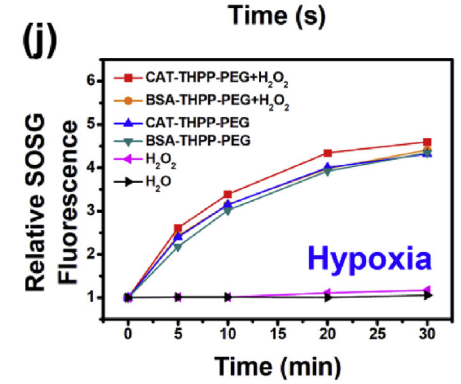

Fig. 1. Preparation and characterization of CAT-THPP-PEG. (a) Schematic illustration of the preparation and structure of CAT-THPP-PEG. (b) Hydrodynamic diameters of catalase, BSA-THPP-PEG and CAT-THPP-PEG in water, PBS and FBS. (c) A TEM image of CAT-THPP-PEG in aqueous. (d) Oxygen generation in H_2O_2 solutions added with different concentrations of CAT-THPP-PEG. (e) Oxygen generation in H_2O_2 solutions with different pH values. (f) Dissolved oxygen content after light illumination. (g) Oxygen generation in H_2O_2 with or without light illumination. (h) The relative enzymatic activity changes of free catalase and CAT-THPP-PEG after protease K digestion for different periods of time. (i&j) Generation of singlet oxygen from CAT-THPP-PEG or BSA-THPP-PEG under normoxic condition (i) and hypoxic condition (j), in the presence or absence of H_2O_2, by measuring the SOSG fluorescence under the 660-nm LED light illumination.

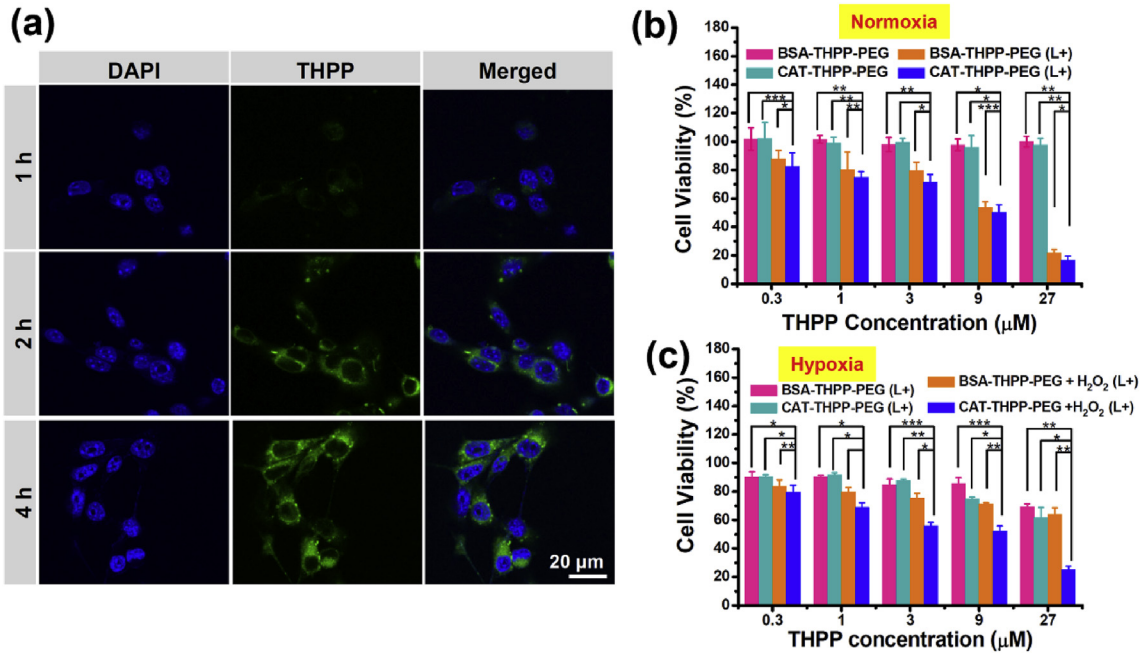

Fig. 2. *In vitro* intracellular internalization and cytotoxicity of CAT-THPP-PEG. (a) Confocal fluorescence micrographs of 4T1 cells after incubation with CAT-THPP-PEG for different periods of time. The scale bar is 20 μm. (b) *In vitro* relative viabilities of 4T1 cells treated with CAT-THPP-PEG or BSA-THPP-PEG under normoxia atmosphere for 24 h. Error bars were based on triplicated samples. (c) *In vitro* relative viabilities of 4T1 cells treated with CAT-THPP-PEG or BSA-THPP-PEG under hypoxia atmosphere and light illumination, with or without addition of H_2O_2. 'L+' indicates 660-nm LED light illumination for 30 min. P values:***$p < 0.001$, **$p < 0.01$, or *$p < 0.05$.

4T1 cells were tested under incubation within a hypoxic atmosphere (5% CO_2, 94% N_2, 1% O_2). Exogenous H_2O_2 (100 μM) was added to mimic the tumor microenvironment for 4 h co-incubation before light illumination. After illumination by a 660-nm LED light at the power density of 5 mW cm^{-2}, cells were transferred into the fresh medium under standard normoxic atmosphere for another 24 h before the followed cell viability assay. As shown in Fig. 2c, due to the additional oxygen generated from the CAT-triggered decomposition of H_2O_2, the PDT-induced cell killing was dramatically enhanced for CAT-THPP-PEG but not for BSA-THPP-PEG under the hypoxic condition.

Owing to the coordination capability of THPP with different types of metal ions, this synthesized CAT-THPP-PEG may be labeled with radioactive metal ions for positron emission tomography (PET) imaging as well as single-photon emission computed tomography (SPECT) without using any other chelators [47]. Herein, ^{99m}Tc with γ-ray emission was directly incorporated inside the porphyrin ring to enable quantitative tracking of in vivo behaviors of labeled nanoparticles by SPECT imaging (Fig. 3a). Typically, technetium-99 m in the $^{99m}TcO_4^-$ form was reduced by $SnCl_2$ into $^{99m}Tc^{4+}$ and added into CAT-THPP-PEG solution. After gentle stirring for 1 h at room temperature, the obtained CAT-THPP(^{99m}Tc)-PEG was purified by ultrafiltration to remove free ^{99m}Tc (labeling yield: 94%). Such CAT-THPP(^{99m}Tc)-PEG exhibited great labeling stability under incubation in FBS at 37 °C (Fig. S4a in supporting information), allowing reliable in vivo tracking of those nanoparticles. Afterwards, the in *vivo* SPECT imaging was performed on 4T1-tumor bearing mice after i. v. injection of CAT-THPP (^{99m}Tc)-PEG (1 mCi). The tumor contrast gradually increased over time, with strong radioactivity signals detected within the tumor at 24 h post-injection (p.i.) (Fig. 3b), suggesting the efficient tumor homing ability of those nanoparticles. Quantitative data obtained from region-of-interest (ROI) analysis of the SPECT images (Fig. 3c) further illustrated that the liver uptake of nanoparticles was gradually decreased from 24.3 ± 2.1% to 17.4 ± 2.7% while the accumulation in tumor was clearly increased from 0.1 ± 0.1% to 5.2 ± 1.7% from 0.5 h to 24 h p. i. The decline of CAT-THPP(^{99m}Tc)-PEG signals in the liver may be due to the basolateral uptake and canalicular export [48,49]. In addition, the quantitative analysis of blood circulation and biodistribution profiles of CAT-THPP(^{99m}Tc)-PEG was studied by measuring the radioactivities of ^{99m}Tc in blood samples as well as main tissues and organs by a gamma counter. As shown in Fig. 3d, CAT-THPP(^{99m}Tc)-PEG nanoparticles exhibited greatly prolonged blood circulation, with the blood half-life determined to be ≈ 6.42 h. In addition, consistent with SPECT imaging photographs, an effective tumor accumulation of CAT-THPP(^{99m}Tc)-PEG was measured to 6.03 ± 1.78% ID g^{-1}, which could attributed to the enhanced permeability and retention (EPR) of tumors to allow passive homing of nanoparticles with long blood circulation half-lives (Fig. 3e).

As reported in the previous work, catalase owns the catalytic ability to decompose tumor endogenous H_2O_2 into O_2 so as to improve the tumor oxygenation [21]. To study the tumor hypoxia status, mice bearing 4T1 tumors were i. v. injected with BSA-THPP-PEG or CAT-THPP-PEG and sacrificed at 24 h post injection to collect tumors for immunofluorescence staining. For the tumor slices, cell nuclei, blood vessels, and hypoxia areas were stained with DAPI (blue), anti-CD31 antibody (red), and antipimonidazole antibody (green), respectively (Fig. 4a). Compared with tumor sections for untreated mice and BSA-THPP-PEG treated mice, whose tumors showed large hypoxia areas, the hypoxia-associated green fluorescence signals for the tumor section from CAT-THPP-PEG injected group showed remarkable decrease, indicating the greatly relieved tumor hypoxia by treatment of CAT-THPP-PEG. Meanwhile, the immunofluorescence staining of HIF-1α using anti-HIF-1α antibody was also conducted for tumor slices (Fig. 4b). Greatly reduced HIF-1α expression was also observed for tumors on mice treated by CAT-THPP-PEG in comparison to the untreated group as well as BSA-THPP-PEG treated group, also evidencing the effective tumor hypoxia relief ability of CAT-THPP-PEG nanoparticles. Semi-quantitative statistical analysis of hypoxia positive areas further confirmed that the tumor hypoxia was successfully reduced by i. v. injection of CAT-encapsulated CAT-THPP-PEG nanoparticles (Fig. 4c). After that, a H_2O_2-responsive probe reported in our previous report [50] was employed to detect H_2O_2 levels in the tumor by photoacoustic imaging (Fig. S3, Supporting Information). Greatly reduced H_2O_2 content in the

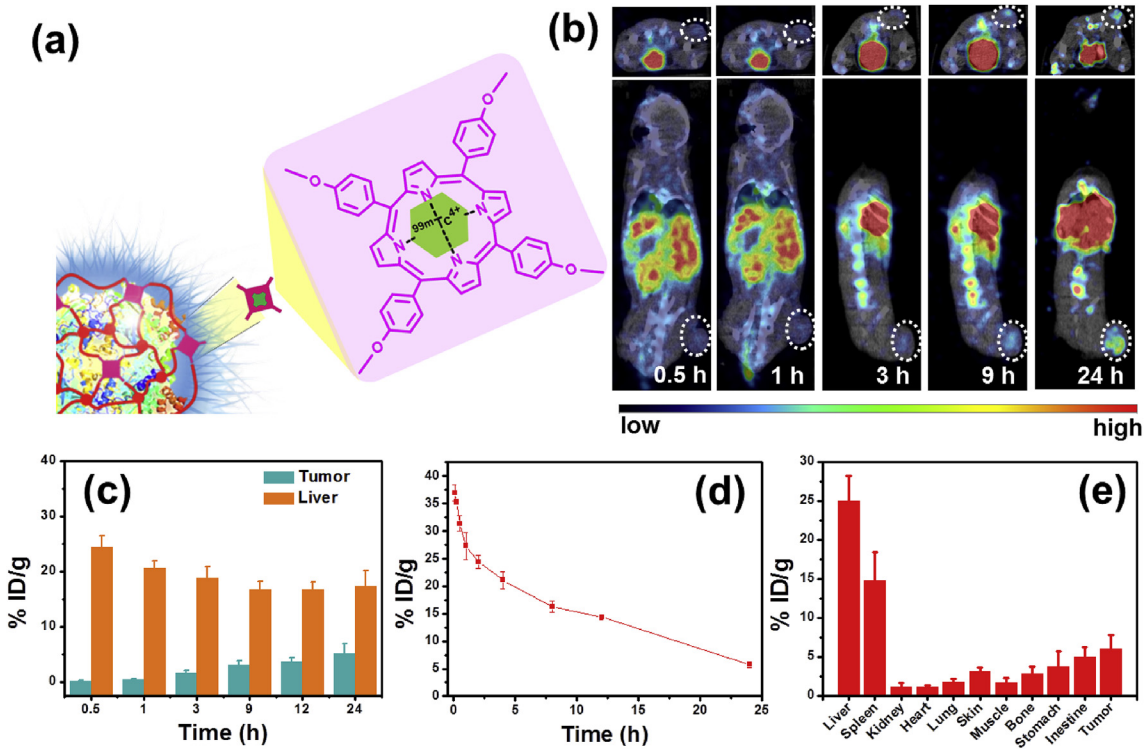

Fig. 3. *In vivo* SPECT imaging and pharmacokinetics of CAT-THPP(^{99m}Tc)-PEG. (a) Schematic illustration of ^{99m}Tc radiolabeling of CAT-THPP-PEG. (b) SPECT images of 4T1 tumor-bearing mice after i. v. injection with CAT-THPP(^{99m}Tc)-PEG. The tumor side was highlighted in the dash circle. (c) Quantitative analysis of the SPECT data. Time-dependent radioactivity changes in the liver and 4T1 tumor upon injection of CAT-THPP(^{99m}Tc)-PEG were presented. (d) The blood circulation of CAT-THPP(^{99m}Tc)-PEG in tumor-bearing mice. (e) Biodistribution of CAT-THPP(^{99m}Tc)-PEG measured at 24 h post i. v. injection.

tumor was observed after the i. v. injection of CAT-THPP-PEG nanoparticles, also indicating the effective in vivo decomposition of tumoral endogenous H_2O_2 by CAT-THPP-PEG.

Next, the in vivo PDT efficacy was evaluated with the 4T1 mouse tumor model. Nude mice bearing 4T1 tumors were randomly divided into four groups (six mice per group) including: (1) PBS, (2), BSA-THPP-PEG plus light, (3) CAT-THPP-PEG, and (4) CAT-THPP-PEG plus light, at the corresponding THPP dose of 8 mg kg^{-1}. At 24 h post injection, mice in group 2 and 4 were irradiated using a 660-nm LED light at the power density of 5 mW cm^{-2} for 1 h. After 5 days, the second round of injection was carried out with the same nanoparticle and optical doses. After receiving various treatments, the tumor sizes were measured by a digital caliper. While PDT with BSA-THPP-PEG could partly inhibit the tumor growth, especially in the first week post treatment, tumors in this group of mice regained their rapid growth speed later on, likely owing to the PDT resistance for tumor cells located in the hypoxic region of those tumors. In contrast, CAT-THPP-PEG injection plus light illumination demonstrated a remarkable inhibitory effect to the tumor growth. Such enhanced PDT could be attributed to the improved tumor oxygenation with the help of CAT to decompose the tumor endogenous H_2O_2, so as to overcome PDT resistance for cancer cells located in hypoxic regions of those tumors (Fig. 4d). Notably, the tumor growth of non-illuminated CAT-THPP-PEG group was also partly suppressed. This phenomenon may be explained by the fact that the relief of tumor hypoxia may lead to the alternated immune-suppressive tumor microenvironment, such as the polarization of tumor-associated macrophages (TAMs) from the immune-suppressive M2 phenotype to the immune-supportive M1 phenotype, so as to favor the anti-tumor immunities [51]. Moreover, the microscopy images of hematoxylin and eosin (H&E) stained tumor slices further confirmed that the PDT treatment in group 4 with CAT-THPP-PEG plus light exposure resulted in the most severe damages to tumor cells (Fig. 4e), to a level much more significant compared to all other control groups.

The potential toxic side effect of CAT-THPP-PEG to mice was then investigated by histological examination of main organs collected from different groups of mice. As shown by micrographs of H&E stained organ slices (Fig. S4c in supporting information), for CAT-THPP-PEG plus illumination group, no obvious histological abnormality could be found in comparison with those collected from the control group. Meanwhile, neither apparent body weight drop nor unexpected mouse death was noted for group 4 (Fig. S4b in supporting information), further suggesting the absence of acute toxicity for such CAT-THPP-PEG nanoparticles. On the other hand, the phototoxicity on skin was also studied by H&E staining of skin slices (Fig. S5 in supporting information), from which one could find that at 24 h post i. v. injection of nanoparticles, no obvious damage on skin could be observed.

As an exogenous protein, the unwanted immunogenicity of catalase may be an important concern for its in vivo use. Therefore, the CAT-specific antibody titer and the tumor necrosis factor (TNF-α) level in cytokine of mice treated with free catalase or CAT-THPP-PEG was determined using enzyme linked immunosorbent assay (ELISA). As shown in Fig. 4f and g, free CAT injection would indeed induce a high CAT-specific antibody titer and TNF-α level, indicating the strong immunogenicity of free CAT. In marked contrast, the titer of CAT-specific IgG or TNF-α level from the CAT-THPP-PEG treated group at the same CAT dose was greatly reduced. Therefore, our CAT-THPP-PEG formulation shows largely diminished immunogenicity, likely owing to the crosslinked PEG shell on the surface of CAT to prevent its direct interaction with the immune-related proteins. This unique advantage would be greatly useful for the potential application of our nanoparticles for in vivo applications upon systemic administration.

3. Conclusion

In this work, we have developed a new class of catalase encapsulated nanoparticles via an in situ free radical polymerization

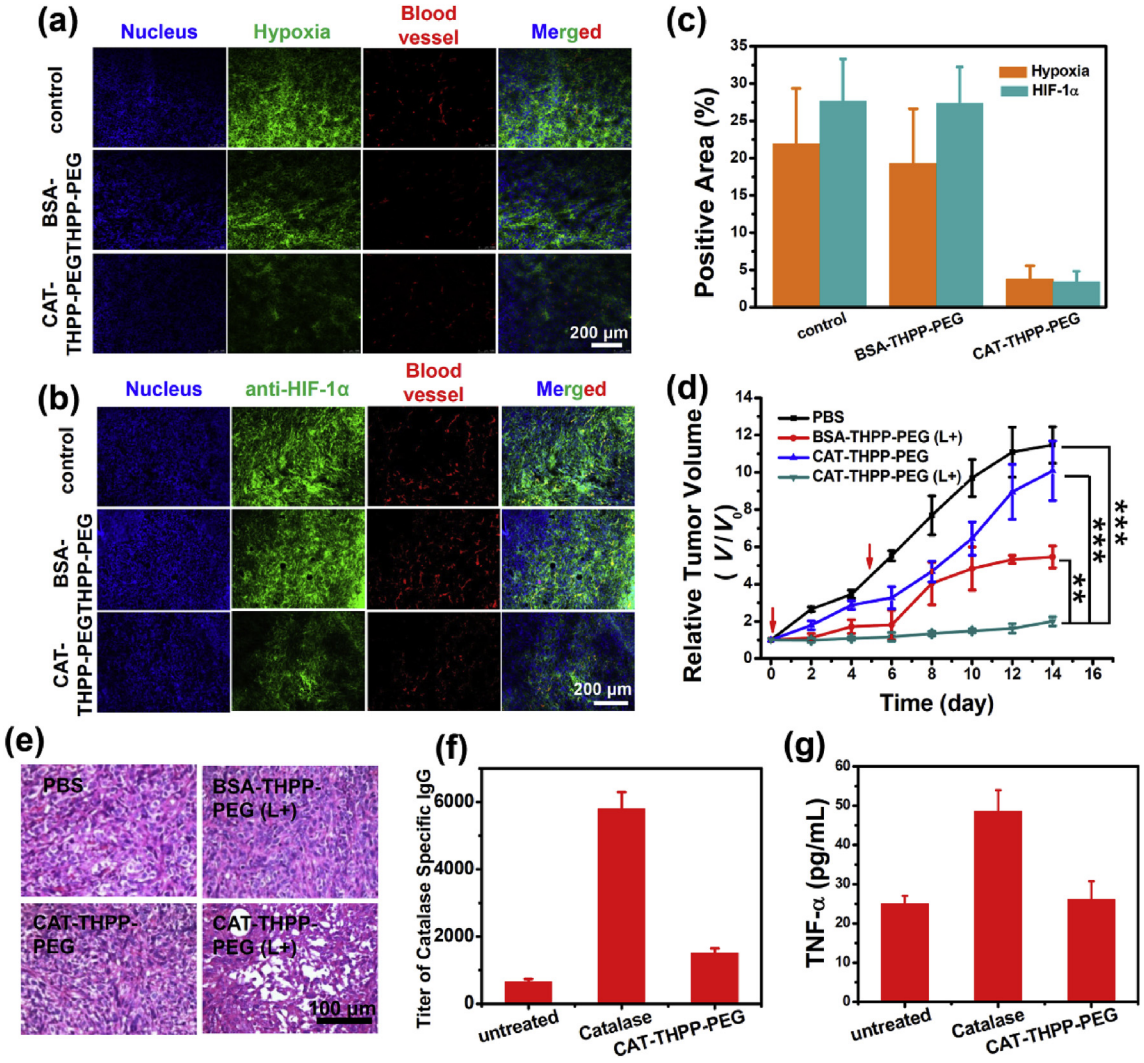

Fig. 4. *In vivo* PDT treatment. (a) Immunofluorescence staining micrographs of tumor slices after treatment with saline, CAT-THPP-PEG or BSA-THPP-PEG. The cell nuclei, blood vessels, and hypoxia areas were stained by DAPI (blue), anti-CD31 antibody (red), and antipimonidazole antibody (green), respectively. (b) Micrograph images of tumor slices with HIF-1α immunofluorescence staining. (c) The quantitative analysis data of hypoxia positive areas as recorded from > 10 micrographs for each group using the Image J software. (d) Tumor growth curves of mice after various different treatments as indicated (THPP dose = 8 mg kg^{-1}, protein dose = 10 mg kg^{-1}) at day 0 and day 5. V_0 and V stood for the tumor volumes before and after the treatment, respectively. (e) Micrographs of H&E stained tumor slices collected from mice of different groups at 24 h after light illumination. (f&g) The titer of catalase-specific antibody (f) and TNF-α levels (g) in mouse serum samples measured 5 days after i. v. injection of free catalase or CAT-THPP-PEG (catalase dose = 10 mg kg^{-1}) as determined by the ELISA assay. P values:***p < 0.001, **p < 0.01, or *p < 0.05. (For interpretation of the references to color in this figure legend, the reader is referred to the Web version of this article.)

method on the surface of catalase under a mild condition. By protecting catalase inside the CAT-THPP-PEG nanoparticles, the enzyme activity and stability of catalase could be well protected. Those CAT-THPP-PEG nanoparticles after labeling with ^{99m}Tc upon simple mixing could be tracked by in vivo SPECT imaging, which illustrated the efficient tumor passive homing of CAT-THPP-PEG with prolonged blood circulation via the EPR effect. Meanwhile, CAT-THPP-PEG accumulated in the tumor could catalyze the tumor endogenous H_2O_2 to produce O_2, which is helpful to relieve tumor hypoxia and enhance the efficacy of oxygen-dependent PDT. Important, those CAT-THPP-PEG nanoparticles without any appreciable in vivo acute toxicity, showed greatly reduced immunogenicity compared to free catalase, an exogenous enzyme, owing to safeguard from the brush-like polymer shell. Therefore, this work presents an innovative approach to fabricate enzyme entrapped nanocapsules by using photosensitizer as the crosslinker to simultaneously achieve different aims by one reaction. Such CAT-THPP-PEG nanoparticles with great enzyme stability and largely reduced immunogenicity enable in vivo SPECT imaging, tumor hypoxia relief, as well as enhanced cancer PDT, and thus would be a rather attractive type of cancer theranostic nanoscale platform.

4. Materials and methods

4.1. Materials

Meso-tetra(*p*-hydroxyphenyl)porphine (THPP), acryloyl chloride and N,N,N′,N′-tetramethylethylenediamine (TEMED) were purchased from J&K Chemical Co. and used as received. N,N′-methylene bis-acrylamide (BIS) was obtained from Alfa Aesar and used directly. Poly (ethylene glycol) methacrylate (PEGMA, $M_n \approx 500$ g mol^{-1}, Sigma-Aldrich) was passed through a column of neutral Al_2O_3 to remove the inhibitors, and stored under N_2 atmosphere at 4 °C. Catalase (CAT) solution (≥35,000 units/mg protein) was purchased from Aladdin. Tetrahydrofuran (THF, AR) was dried over KOH for at least two days and then refluxed over a sodium wire with benzophenone as an indicator until the color turned to purple. Triethylamine (TEA, Sinopharm Chemical Reagent) were distilled before use. The other reagents and solvents were purchased from Sinopharm Chemical Reagent and used

as received.

4.2. Synthesis of meso-tetra(p-acryloylphenyl)porphine, acryloyl-THPP

Acryloyl-THPP was synthesized by nucleophilic substitution between meso-tetra(*p*-hydroxyphenyl) porphine (THPP) and acryloyl chloride. Briefly, THPP (135.6 mg, 0.2 mmol) and triethylamine (TEA, 240.9 mg, 2.4 mmol) were dissolved in 50 mL of anhydrous tetrahydrofuran (THF) and then acryloyl chloride (222.7 mg, 2.4 mmol) was added dropwisely into the solution over 30 min at 0 °C. After stirring for 12 h under nitrogen (N_2) atmosphere at 25 °C, the triethylamine hydrochloride was removed by filtration and the solvent was concentrated by rotary evaporation. The crude product was re-dissolved in dichloromethane and washed with 0.1 M Na_2CO_3 aqueous solution/distilled water subsequently for five times followed by drying with anhydrous $MgSO_4$ for 2 h. Afterwards, the solution was concentrated and precipitated into 30 mL of cold hexane, filtered and dried under vacuum at 30 °C for 24 h to obtain meso-tetra(p-acryloylphenyl)porphine (acryloyl-THPP) as the dark purple powder. The chemical structure was characterized by ^{1}H NMR spectrum (Bruke, 400 MHz).

4.3. Synthesis of CAT-THPP-PEG and BSA-THPP-PEG

Catalase (CAT) was modified by reacting its surface amino group with N-acryloxysuccinimide (NAS) and followed by in situ free radical polymerization. Typically, 200 μL of CAT solution (10 mg mL^{-1}) or 2 mg bovine serum albumin (BSA) was mixed with 19.6 mg NAS dissolved in 7 mL of 50 mM HEPES buffer solution (pH = 8.5). The acryloylation was taken place under 4 °C for 3 h. After that, 500 μL of N,N-dimethylformamide (DMF) containing 1.2 mg acryloyl-THPP, N,N′-methylene bis-acrylamide (BIS, 2 mg), poly(ethylene glycol) methacrylate (PEGMA, 150 mg), ammonium persulfate (APS, 30 mg) and N,N,N′,N′-tetramethylethylenediamine (TEMED, 30 mg) were subsequently added to the acrylated CAT. The mixture was stirred at 4 °C for another 3 h. After that, the resulting solution was dialyzed against 50 mM HEPES buffer (pH = 8.5) at 4 °C remove the unreacted monomers and initiators, followed by a further purification by gel filtration with Sephacryl S-300 HR to remove free enzymes.

4.4. Characterization of the CAT-THPP-PEG

The concentration of THPP was determined by UV–Vis spectra (Genesys 10s, Thermo Scientific, USA). The morphologies of the nanoparticles were observed on a TEM instrument (TECNAI G2) while the hydrodynamic sizes of nanoparticles were measured by ZEN3690 zetasizer (Malvern, USA). The singlet oxygen generation was detected according to the previously literature [52,53] by using the SOSG as the fluorescence probe. The dissolved oxygen concentration in aqueous solution was determined using a portable dissolved oxygen meter (Rex, JPBJ-608, China) to evaluate the catalysis capability of CAT-THPP-PEG.

4.5. Catalase activity assay

Catalase activity was determined by the Góth method [45]. Briefly, 1 mL of hydrogen peroxide (50 mM) was added with 0.2 mL of free catalase or CAT-THPP-PEG (0.5 μM) for 1 min at 37 °C, and the catalytic reaction was terminated by adding 1 mL of ammonium molybdate (32.4 mM) and cooling down to 25 °C. Since ammonium molybdate could react with the residual H_2O_2 to form primrose stable complexes, the catalase activity could be determined by detecting the absorbance of the formed complex at 400 nm. To measure the stability of catalase, both free catalase and CAT-THPP-PEG were incubated with protease K (0.4 mg mL^{-1}) at 37 °C. At predetermined time points, aliquots of sample were removed and cooled down to 25 °C for immediate catalase activity assay.

4.6. In vitro cellular internalization of CAT-THPP-PEG

To investigate the cellular internalization behavior of CAT-THPP-PEG, 4T1 cells seeded in 24-well plates were with CAT-THPP-PEG ([THPP] = 8 μM) for different periods of time (1 h, 2 h, 4 h and 8 h). After that, all samples were washed with fresh PBS for 3 times and the cells were labeled with 4,6-diamino-2-phenylindole (DAPI) before confocal imaging (LeciaSP5 laser scanning confocal microscope). The fluorescence of THPP was collected with the excitation wavelength at 633 nm and the emission wavelength from 660 nm to 750 nm.

4.7. Cytotoxicity of CAT-THPP-PEG

To study the *in vitro* therapeutic effects of synthesized CAT-THPP-PEG nanoparticles, the standard thiazolyltetrazolium (MTT, Sigma Aldrich) assay method was employed. Typically, 4T1 cells seeded in 96-well plates were cultured under nitrogen atmosphere using a hypoxic cell incubator (5% CO_2, 94% N_2, 1% O_2) with various concentrations of CAT-THPP-PEG or BSA-THPP-PEG for 4 h. After that, H_2O_2 (100 μM) were added and then the 96-well plates were exposed to 660 nm light at a power density of 5 mW cm^{-2} for 30 min. Then, the cells were incubated in fresh medium for 24 h. Finally, the relative cell viabilities were determined by the MTT assay.

4.8. Animals

Balb/c mice were purchased from Nanjing Peng Sheng Biological Technology Co. Ltd. and used under protocols approved by Soochow University Laboratory Animal Center. All the intravenous (i.v.) injection was treated by tail vein.

^{99m}Tc Labeled CAT-THPP-PEG for SPECT Imaging: For ^{99m}Tc labeling of CAT-THPP-PEG, 2 mCi of technetium-99 m in the $^{99m}TcO_4^-$ form (purchased from Shanghai GMS Pharmaceutical Co., Ltd) was added into 200 μL of CAT-THPP-PEG solution ([THPP] = 1 mg mL^{-1}) in the presence of 100 μL of $SnCl_2$ (10 mg mL^{-1} in 0.1 M HCl), which would reduce $^{99m}TcO^{4-}$ into $^{99m}Tc^{4+}$. After gentle stirring for 1 h at room temperature, the obtained CAT-THPP(^{99m}Tc)-PEG was purified by ultrafiltration to remove free ^{99m}Tc. For radiolabeling stability test, CAT-THPP(^{99m}Tc)-PEG was incubated in serum at 37 °C for different periods of time (0.5, 1, 4, 8, 12 and 24 h). The released ^{99m}Tc from CAT-THPP (^{99m}Tc)-PEG was collected by ultrafiltration for gamma counting. For Single-Photon Emission Computed Tomography (SPECT) imaging, mice bearing 4T1 tumors were imaged by in vivo animal SPECT (MILabs, Utrecht, the Netherlands) imaging system at different time points post i. v. injection of CAT-THPP(^{99m}Tc)-PEG (500 μCi per mouse). For in vivo pharmacokinetic studies, three 4T1-tumor bearing mice were i. v. injected with CAT-THPP(^{99m}Tc)-PEG (500 μCi per mouse). After that, blood sample was collected at different time intervals, weighed, and then measured by the gamma counter to determine the radioactivity levels in the blood. After 24 h, those mice were sacrificed and their organs including heart, liver, spleen, lung, kidney, skin, muscle, bone, and tumor were taken, weighed and measured by the gamma counter. Decay half-life correction was performed when analyzing the above time-dependent data.

4.9. Immunofluorescent staining

4T1 tumor-bearing mice were i. v. injected with PBS, BSA-THPP-PEG or CAT-THPP-PEG (THPP dose = 8 mg kg^{-1}). Immunofluorescence staining of tumor slices were conducted for tumors collected at 24 h post injection, following a well-established protocol [21]. The immunofluorescence staining images were captured by a confocal microscopy (Leica SP5). Image intensity quantification of tumor hypoxia was performed with the ImageJ software. The hypoxic positive area (%) = visible hypoxic marker in tumor tissue section/total area (n = 10/group).

4.10. In vivo combined therapy

Nude mice bearing 4T1 tumors were randomly divided into four groups with six mice per group: (1) PBS, (2), BSA-THPP-PEG plus light, (3) CAT-THPP-PEG, and (4) CAT-THPP-PEG plus light, at the corresponding THPP dose of 8 mg kg^{-1}. At 24 h post injection, mice in group 2 and 4 were irradiated using a 660-nm LED light at the power density of 5 mW cm^{-2} for 1 h. After 5 days, the second round of treatment was carried out with the same THPP and optical doses. The tumor size and body weight were monitored every two days for 14 days and the tumor volume was calculated according to the following formula: $width^2 \times length/2$. Main organs (liver, spleen, kidney, heart, and lung) of each group after 14 days treatment as well as the tumor tissue harvested from one mouse of each group after 24 h p. i. were collected for hematoxylin and eosin (H&E) staining.

4.11. Enzyme linked immunosorbent assay (ELISA)

Nine female Balb/c mice were randomly divided into three groups and intravenously injected with PBS, free catalase or CAT-THPP-PEG (catalase does = 10 mg kg^{-1}). After 5 days, the titer of catalase-specific IgG in sera and TNF-α in cytokine isolated from mice was analyzed using ELISA assay according to vendors' protocols. The end-point titer of the antibody was defined as the reciprocal of the highest dilution at which the absorption intensity was above the mean + 4 standard deviation (SD) of that of the serum samples from PBS treated mice [54].

Acknowledgements

This article was partially supported by the National Basic Research Programs of China (973 Program) (2016YFA0201200), the National Natural Science Foundation of China (51525203, 51761145041), Collaborative Innovation Center of Suzhou Nano Science and Technology, and a Project Funded by the Priority Academic Program Development (PAPD) of Jiangsu Higher Education Institutions.

Appendix A. Supplementary data

Supplementary data related to this article can be found at https://doi.org/10.1016/j.biomaterials.2018.08.011.

References

[1] J.M. Brown, W.R. Wilson, Nat. Rev. Canc. 4 (2004) 437–447.
[2] Z.F. Yang, R.T. Poon, J. To, D.W. Ho, S.T. Fan, Canc. Res. 64 (2004) 5496–5503.
[3] M. Matsuo, S. Matsumoto, J.B. Mitchell, M.C. Krishna, K. Camphausen, Semin. Radiat. Oncol. 24 (2014) 210–217.
[4] I. Lohse, C. Lourenco, E. Ibrahimov, M. Pintilie, M.-S. Tsao, D. Hedley, Cancers 6 (2014) 459–471.
[5] J.M. Brown, A.J. Giaccia, Canc. Res. 58 (1998) 1408–1416.
[6] M.A. Swartz, N. Iida, E.W. Roberts, S. Sangaletti, M.H. Wong, F.E. Yull, L.M. Coussens, Y.A. DeClerck, Canc. Res. 72 (2012) 2473–2480.
[7] R. Kumar, E.-J. Kim, J. Han, H. Lee, W.S. Shin, H.M. Kim, S. Bhuniya, J.S. Kim, K.S. Hong, Biomaterials 104 (2016) 119–128.
[8] C.-C. Huang, W.-T. Chia, M.-F. Chung, K.-J. Lin, C.-W. Hsiao, C. Jin, W.-H. Lim, C.-C. Chen, H.-W. Sung, J. Am. Chem. Soc. 138 (2016) 5222–5225.
[9] W.P. Fan, W.B. Bu, J.L. Shi, Adv. Mater. 28 (2016) 3987–4011.
[10] Y. Yuan, C.-J. Zhang, R.T.K. Kwok, S. Xu, R. Zhang, J. Wu, B.Z. Tang, B. Liu, Adv. Funct. Mater. 25 (2015) 6586–6595.
[11] H. Gong, Y. Chao, J. Xiang, X. Han, G.S. Song, L.Z. Feng, J.J. Liu, G.B. Yang, Q. Chen, Z. Liu, Nano Lett. 16 (2016) 2512–2521.
[12] L.Z. Feng, L. Cheng, Z.L. Dong, D.L. Tao, T.E. Barnhart, W.B. Cai, M.W. Chen, Z. Liu, ACS Nano 11 (2017) 927–937.
[13] W.P. Fan, W.B. Bu, B. Shen, Q.J. He, Z.W. Cui, Y.Y. Liu, X.P. Zheng, K.L. Zhao, J.L. Shi, Adv. Mater. 27 (2015) 4155–4161.
[14] C.R. Gordijo, A.Z. Abbasi, M.A. Amini, H.Y. Lip, A. Maeda, P. Cai, P.J. O'Brien, R.S. DaCosta, A.M. Rauth, X.Y. Wu, Adv. Funct. Mater. 25 (2015) 1858–1872.
[15] W.W. Zhu, Z.L. Dong, T.T. Fu, J.J. Liu, Q. Chen, Y.G. Li, R. Zhu, L.G. Xu, Z. Liu, Adv. Funct. Mater. 26 (2016) 5490–5498.
[16] X. Yi, L. Chen, X.Y. Zhong, R.L. Gong, Y.T. Qian, F. Wu, G.S. Song, Z.F. Chai, Z. Liu, K. Yang, Nano Res. 9 (2016) 3267–3278.
[17] Q. Chen, L. Feng, J. Liu, W. Zhu, Z. Dong, Y. Wu, Z. Liu, Adv. Mater. 28 (2016) 7129–7136.
[18] H.C. Chen, J.W. Tian, W.J. He, Z.J. Guo, J. Am. Chem. Soc. 137 (2015) 1539–1547.
[19] F. Caruso, D. Trau, H. Möhwald, R. Renneberg, Langmuir 16 (2000) 1485–1488.
[20] Y.J. Wang, F. Caruso, Chem. Commun. (2004) 1528–1529.
[21] Q. Chen, J. Chen, C. Liang, L. Feng, Z. Dong, X. Song, G. Song, Z. Liu, J. Contr, Release 263 (2016) 79–89.
[22] G.S. Song, Y.Y. Chen, C. Liang, X. Yi, J.J. Liu, X.Q. Sun, S.D. Shen, K. Yang, Z. Liu, Adv. Mater. 28 (2016) 7143–7148.
[23] Y. Zhang, B. Heym, B. Allen, D. Young, S. Cole, Nature 358 (1992) 591–593.
[24] H. Aebi, Methods Enzymol. 105 (1984) 121–126.
[25] S. Schoffelen, J.C.M. van Hest, Soft Matter 8 (2012) 1736–1746.
[26] J. Xie, S. Lee, X.Y. Chen, Adv. Drug Deliv. Rev. 62 (2010) 1064–1079.
[27] W. Wang, Y. Xu, D.I.C. Wang, Z. Li, J. Am. Chem. Soc. 131 (2009) 12892–12893.
[28] H. Ai, S.A. Jones, Y.M. Lvov, Cell Biochem. Biophys. 39 (2003) 23.
[29] O.I. Wilner, Y. Weizmann, R. Gill, O. Lioubashevski, R. Freeman, I. Willner, Nat. Nanotechnol. 4 (2009) 249–254.
[30] Y. Liu, J. Du, M. Yan, M.Y. Lau, J. Hu, H. Han, O.O. Yang, S. Liang, W. Wei, H. Wang, J. Li, X. Zhu, L. Shi, W. Chen, C. Ji, Y. Lu, Nat. Nanotechnol. 8 (2013) 187–192.
[31] F.G. Sheikh, K. Pahan, M. Khan, E. Barbosa, I. Singh, P Natl. Acad. Sci. USA 95 (1998) 2961–2966.
[32] G. Stempfer, B. HollNeugebauer, E. Kopetzki, R. Rudolph, Nat. Biotechnol. 14 (1996) 481–484.
[33] C.P. Govardhan, Curr. Opin. Biotechnol. 10 (1999) 331–335.
[34] P. Wang, M.V. Sergeeva, L. Lim, J.S. Dordick, Nat. Biotechnol. 15 (1997) 789–793.
[35] Z. Yang, D. Williams, A.J. Russell, Biotechnol. Bioeng. 45 (1995) 10–17.
[36] Z. Yang, A.J. Mesiano, S. Venkatasubramanian, S.H. Gross, J.M. Harris, A.J. Russell, J. Am. Chem. Soc. 117 (1995) 4843–4850.
[37] M. Yan, J. Ge, Z. Liu, P.K. Ouyang, J. Am. Chem. Soc. 128 (2006) 11008–11009.
[38] M. Yan, J.J. Du, Z. Gu, M. Liang, Y.F. Hu, W.J. Zhang, S. Priceman, L.L. Wu, Z.H. Zhou, Z. Liu, T. Segura, Y. Tang, Y.F. Lu, Nat. Nanotechnol. 5 (2010) 48–53.
[39] H. Lee, J.H. Jeong, T.G. Park, J. Contr. Release 79 (2002) 283–291.
[40] S. Katayose, K. Kataoka, Bioconjugate Chem. 8 (1997) 702–707.
[41] A. Sato, S.W. Choi, M. Hirai, A. Yamayoshi, R. Moriyarna, T. Yamano, M. Takagi, A. Kano, A. Shimamoto, A. Maruyama, J. Contr. Release 122 (2007) 209–216.
[42] A. Rastogi, S. Nad, M. Tanaka, N. Da Mota, M. Tague, B.A. Baird, H.D. Abruna, C.K. Ober, Biomacromolecules 10 (2009) 2750–2758.
[43] N. Li, H. Cai, L. Jiang, J.N. Hu, A. Bains, J. Hu, Q.Y. Gong, K. Luo, Z. Gu, ACS Appl. Mater. Interfaces 9 (2017) 6865–6877.
[44] H.Y. Huang, R. Hernandez, J.M. Geng, H.T. Sun, W.T. Song, F. Chen, S.A. Graves, R.J. Nickles, C. Cheng, W.B. Cai, J.F. Lovell, Biomaterials 76 (2016) 25–32.
[45] L. Góth, Clin. Chim. Acta 196 (1991) 143–151.
[46] T. Wen, H. Zhang, Y. Chong, W.G. Wamer, J.J. Yin, X.C. Wu, Nano Res. 9 (2016) 1663–1673.
[47] L. Cheng, D.W. Jiang, A. Kamkaew, H.F. Valdovinos, H.-J. Im, L.Z. Feng, C.G. England, S. Goel, T.E. Barnhart, Z. Liu, W.B. Cai, Adv. Funct. Mater. 27 (2017) 1702928–n/a.
[48] P.B. Olthof, R.F. van Golen, B. Meijer, A.A. van Beek, R.J. Bennink, J. Verheij, T.M. van Gulik, M. Heger, Biochim. Biophys. Acta (BBA) - Mol. Basis Dis. 1863 (2017) 375–385.
[49] M.J. Reiniers, R.F. van Golen, S. Bonnet, M. Broekgaarden, T.M. van Gulik, M.R. Egmond, M. Heger, Anal. Chem. 89 (2017) 3853–3857.
[50] Y.H. Hu, H.J. Chen, X.Z. Zhao, J.J.X. Wu, F. Muhammad, S.C. Lin, J. He, L.Q. Zhou, C.P. Zhang, Y. Deng, P. Wang, Z.Y. Zhou, S.M. Nie, H. Wei, ACS Nano 11 (2017) 5558–5566.
[51] G.B. Yang, L.G. Xu, Y. Chao, J. Xu, X.Q. Sun, Y.F. Wu, R. Peng, Z. Liu, Nat. Commun. 8 (2017) 902.
[52] Z. Zhu, Z.W. Tang, J.A. Phillips, R.H. Yang, H. Wang, W.H. Tan, J. Am. Chem. Soc. 130 (2008) 10856–10857.
[53] S. Jeong, W. Park, C.-S. Lee, K. Na, Macromol. Biosci. 14 (2014) 1688–1695.
[54] A. Stano, A.J. van der Vlies, M.M. Martino, M.A. Swartz, J.A. Hubbell, E. Simeoni, Vaccine 29 (2011) 804–812.